Atomistic Simulations of Dislocations in a Model BCC Multicomponent Concentrated Solid Solution Alloy

S.I. Rao[,2],[3] C.Varveene[3,4], C.Woodward[,1], T.A.Parthasarathy[2], D.Miracle[1], O. Senkov[2] and W.A. Curtin[3]

[1] Air Force Research Laboratory, Materials and Manufacturing Directorate, WPAFB, OH 45433

[2] UES Inc, 4401 Dayton-Xenia Road, Dayton, OH 45432

[3] Institute of Mechanical Engineering, EPFL, Lausanne 1015

[4] D

Abstract

Molecular statics and molecular dynamics simulations are presented for the structure and glide motion of a/2<111> dislocations in a randomly-distributed model-BCC $Co_{16.67}Fe_{36.67}Ni_{16.67}Ti_{30}$ alloy. Core structure variations along an individual dislocation line are found for a/2<111> screw and edge dislocations. One reason for the core structure variations is the local variation in composition along the dislocation line. Calculated unstable stacking fault energies on the (110) plane as a function of composition vary significantly, consistent with this assessment. Molecular dynamics simulations of the critical glide stress as a function of temperature show significant strengthening, and much shallower temperature dependence of the strengthening, as compared to pure BCC Fe as well as a reference mean-field BCC alloy material of the same lattice and elastic constants of the target alloy. Interpretation of the strength versus temperature in terms of an effective kink-pair activation model shows the random alloy to have a much larger activation energy than the mean-field alloy or BCC Fe. This is interpreted as due to the core structure variations along the dislocation line that are often unfavorable for glide in the direction of the load. The configuration of the gliding dislocation is wavy, and significant debris is left behind, demonstrating the role of local composition and core structure in creating kink pinning (super jogs) and/or deflection of the glide plane of the dislocation.

1.0 Introduction

Recent work has shown that when 5 or more elements are combined in nearly equiatomic concentrations, a new class of materials emerges. These materials are called High Entropy Alloys (HEA) stemming from the idea that entropy of mixing may stabilize novel phases in many-component systems. The number of phases in a HEA system can be significantly smaller than the maximum number of phases present at equilibrium as predicted by the well-known Gibbs phase rule [1]. While many alloys that meet the definition of an HEA [2,3] contain multiple phases, including intermetallics [4,5], there are many single-phase systems [6]. These single-phase systems, both FCC and BCC, generally have unusually high yield strength and/or high ductility. The origin of the strengthening in FCC HEAs has been proposed as due to solute/dislocation interactions, that is solute strengthening in concentrated alloys [7]. The origin of the strengthening in BCC refractory HEAs, which retain significant strength up to very high temperatures [8,9], has been discussed in the framework of the elastic interactions of the crystal lattice (caused by different atomic radii and elastic moduli of the alloying elements) with dislocations [10]. However, BCC materials generally deform plastically by a dislocation kink-pair nucleation mechanism for the screw dislocations, which is very sensitive to the precise screw core structure.Thus, the strengthening may arise from local variations in core structure in these compositionally-complex alloys. In this paper, we use atomistic simulations to investigate the origins of strengthening in a model BCC HEA. We show that the random alloy has a much higher strength than a corresponding "mean-field" material composed of a single atom type but having the same bulk properties of the random alloy. Thus, local compositional disorder is the source of the observed strengthening. We also show that the compositional disorder induces significant variations in local core structure along the length of a single dislocation. The measured strength and measured high effective kink-pair activation energy are hypothesized to be due to the inhibition of dislocation motion due to the core structure variations.

Atomistic modeling of multicomponent metals has been challenging since it requires accurate interatomic potentials for all of the interacting elemental components of the alloy. The literature has thus mainly focused on binary systems, such as Ni-Al and Al-Mg, with very detailed tuning of parameters to achieve quantitative predictive capability. However, a suite of potentials for 16 different metallic elements (Cu, Ag, Au, Ni, Pd, Pt, Al, Pb, Fe, Mo, Ta, W, Mg, Co, Ti, Zr) was developed some years ago [11] with the aim of maintaining a unified description of all

elements such that any combination of these elements could be studied via simulation. The existence of this suite of potentials enables investigation of a very wide scope of possible multicomponent alloys, including High Entropy Alloys. The suite of potentials were fit mainly to elemental properties, and thus properties that were not fit and properties of multicomponent alloys are not assured to be quantitatively accurate. However, the ability to generate model systems of arbitrary complexity presents a huge opportunity to explore and discover mechanisms of deformation in systems where concepts developed for elemental and dilute binary alloys may not apply. Here, we take advantage of these potentials to probe a model BCC HEA material precisely to uncover heretofore unknown mechanisms of plastic deformation. Any new insights into the unusual mechanical behavior of BCC high entropy alloys can be used to guide future alloy discovery.

2. Computational model of the BCC $Co_{16.67}Fe_{36.67}Ni_{16.67}Ti_{30}$ random alloy

A four element Co-Fe-Ni-Ti interatomic potential developed by Zhou et al. [11,12] was implemented in the molecular dynamics (MD) code LAAMPS [13]. An atomistic simulation cell consisting of a BCC lattice with lattice constant 2.86A was created, with periodic boundary conditions along three orthogonal directions x=[1-10], y=[110] and z=[001], with dimensions of ~300A in each direction (~ 2 million atoms). BCC lattice sites were randomly occupied by Co, Fe, Ni, and Ti atoms to achieve an average composition $Co_{16.67}Fe_{36.67}Ni_{16.67}Ti_{30}$. The system was relaxed under NPT conditions at P=0 and T=0 to obtain the minimum-energy lattice parameter of 2.96A for the random alloy. The elastic constants C_{11}, C_{12} and C_{44} for the alloy were determined using standard straining methods, yielding C_{11} = 165.3 GPa, C_{12}=132.5 GPa, and C_{44} = 91.9 GPa. Such values are similar to Fe-36Ni [14].

A second BCC simulation cell was created with the three orthogonal axes along x=[111], y=[11-2], and z=[110], with dimensions of approximately 300A in each direction (~ 2 million atoms). This cell was relaxed using free surface boundary conditions along z and periodic boundary conditions along x and y. The upper half of the simulation cell was then translated with respect to the bottom half the unstable stacking fault vector 1/6[111] and the system was relaxed to equilibrium at P=0 and T=0. A similar procedure was used with the fault vector 1/3[111]. The resulting unstable stacking fault energies were then computed from energy differences to yield $\gamma_{usf}([111]/6)$=385 mJ/m^2 and $\gamma_{usf}([111]/3)$=418 mJ/m^2, values that are comparable to pure V [15].

To assess the compositional dependence of the unstable stacking fault energies, similar simulations were also performed over a range of alloy compositions Co 0.2-0.5, Fe 0.2-0.5, Ni 0.1-0.3, and Ti 0.2-0.4, with the bcc lattice being unstable for Co> 0.4. Figure 1 shows the computed $\gamma_{usf}([111]/3)$ as a function of Fe content, for the various Ti, Co, and Ni concentrations. In general, increasing Co, Ni and Ti concentrations tended to decrease $\gamma_{usf}([111]/3)$ while $\gamma_{usf}([111]/3)$ increased approximately linearly with increasing Fe content. Over the composition space studied, $\gamma_{usf}([111]/3)$ ranged from ~ 380 – 480mJ/m^2. Similar behavior was found for $\gamma_{usf}([111]/6)$. These results indicate that local concentration fluctuations in the model $Co_{16.67}Fe_{36.67}Ni_{16.67}Ti_{30}$ alloy lead to significant local variations in unstable stacking fault energies, which would have an impact on local core structures of dislocations.

To study dislocation structure and dynamics, a ½[111] screw dislocation with line direction x=[111], glide direction y=[11-2], and glide plane normal [-110], was inserted into a cell with the edge lengths of X=300A , Y=1200A , and Z=300A, containing 8 million atoms in total. The dislocation was inserted by deforming the atomic positions according to the anisotropic elastic Volterra solution. Conjugate gradient energy minimization was then performed on the initial atomic positions with periodic boundary conditions along the line direction x and fixed boundary conditions along y and z. Similarly, a ½[111] edge dislocation with the line direction along y=[11-2] was introduced inside a cell with dimensions x=1200A in the glide direction, y=300A, and z=300A. Energy minimization was performed using periodic boundary conditions along x and fixed boundary conditions along y and z. To measure the critical resolved shear stress for motion at 0^{o}K, a pure shear stress was applied (τ_{xz} on the (-110) glide plane) by straining the atoms to a desired fixed shear strain and then holding the boundary atoms along y and z fixed while the remainder of the system was energy minimized. This was repeated for a range of shear stresses. Molecular dynamics simulations were performed to determine the variation of the critical stress required to overcome the solute obstacles as a function of temperature. The initial condition for the MD simulations was a molecular statics relaxed core under the applied stress of interest. The system was permitted to relax under NVT conditions at various temperatures for 100ps. The position of the dislocation was then monitored as a function of time to follow its motion.

Under increasing applied shear load, both the a/2<111> screw and edge dislocations will experience significant local movement prior to the load at which uninterrupted glide occurs. As a

result, the dimension of the cell perpendicular to the dislocation line direction was made large (~1200A) so as to avoid significant image stress effects from the free surfaces.

The Nye tensor [16] is used to visualize cross-sections of the dislocation core structure at various points along the dislocation line. The relaxed configuration of the dislocation-free lattice is used as the initial state. The Nye tensor describes the distribution of Burgers vector across the plane normal to the dislocation line and provides an excellent means of visualizing the spatial variation of the misfit. Differential displacement plots [17] of thin sections along the dislocation line are also used to characterize the core structure of a/2<111> screw dislocations in the model BCC structure for some cases. In the differential displacement plots, each circle is a row of atoms along the dislocation threading direction, and an arrow between two rows of atoms corresponds to the relative displacement between the rows compared with the perfect crystal [16]. The length of the arrow scales as the magnitude of the relative displacement between atom rows.

Direct simulations show the behavior of the dislocation in the true random alloy, but it is difficult to specifically identify the role of local fluctuations in material behavior without an appropriate reference system. To this end, recent work has shown that, for various functional forms of interatomic potentials, an "average atom" (A-atom) interatomic potential can be rigorously constructed for any random alloy composed [18]. Most importantly, the many properties of the true random alloy, such as average lattice constant, elastic constants, and stacking fault energies, are accurately reproduced by the single A-atom potential. Thus, the A-atom interatomic potential is the mean-field representation of the true random alloy, capturing all properties that do not depend on local composition fluctuations in the material. Therefore, comparing the dislocation structure and motion between the true random alloy and the mean-field A-atom for the same alloy allows us to identify if a property is controlled by average properties or fluctuation properties (i.e. local concentration fluctuations). We have created the A-atom potential for the $Co_{16.67}Fe_{36.67}Ni_{16.67}Ti_{30}$ alloy, and have verified that the A-atom potential has essentially the same reference properties as the true random alloy. The A-atom potential gives a bcc lattice parameter of 2.9722A (Random alloy = 2.96A), elastic constants C_{11} = 157 GPa, C_{12} = 118 GPa and C_{44} = 101 GPa (Random alloy: C_{11} = 165 GPa, C_{12} = 133 GPa, C_{44} = 92 GPa), unstable stacking fault energies γ_{usf} ([111/6]) and γ_{usf} ([111/3]) on the (110) plane = 402 mJ/m^2 (Random alloy : γ_{usf} ([111]/6) = 385 mJ/m^2, γ_{usf} ([111]/3) = 418 mJ/m^2). We have also used direct atomistic simulations to determine the volume change due to Co, Fe, Ni and Ti atoms in the average A-atom BCC lattice.

One obtains ΔV values of -2.04, -1.94, -1.63 and 3.92 A^3 for the Co, Fe, Ni and Ti atoms, respectively. This suggests that the Ti atom is a very strong misfit strain center in the model bcc multicomponent alloy whereas Ni, Co and Fe atoms have lower misfit strain values. Therefore, strong lattice distortions are expected around the Ti atoms in the model BCC multicomponent alloy. We have also used this A-atom potential in simulations of both edge and screw dislocations using the geometries and methods described above, and below can make comparisons between the true random alloy and its mean-field A-atom representation.

3. Results

3.1 Core structures of the screw and edge dislocations

Figure 2a shows the Nye tensor plot of the relaxed ½[111] screw dislocation core in the model BCC $Co_{16.67}Fe_{36.67}Ni_{16.67}Ti_{30}$ alloy. The Nye tensor is using three adjacent Burgers vector segments along the dislocation line, only the tensor components of the central segment are shown. The Nye tensor is calculated for 0 and +/- 30b along the dislocation line relative to the center of the simulation cell. The a/2<111> screw dislocation cores are spread on several (110) planes and are non-planar, similar to BCC metals. The center of the core along the y and z directions does not vary significantly from section to section along the dislocation line, but the type and extent of non-planarity varies from section to section along the dislocation line. This suggests that the initial relaxed screw dislocation is almost straight, but with significant core structure variations along the dislocation line, which presumably depends on the local concentration variations along the dislocation line in the random bcc $Co_{16.67}Fe_{36.67}Ni_{16.67}Ti_{30}$ alloy. The fact that the screw dislocation is initially straight is also seen in the top view (z-projection) of the screw dislocation, shown in Figure 2b, where atoms with a coordination number other than the bcc coordination of 14 (2^{nd} neighbor) is shown. There is significant background noise in this plot because of the large lattice distortions in the random alloy. The screw dislocation in the mean-field A-atom material remains perfectly straight, as in any elemental BCC metal, and the differential displacement plot for the core structure is shown in Figure 3 is independent of position along the (straight) line. The differential displacement plot shows a classical 3-fold splitting similar to other monoatomic EAM potentials [19].

Figure 4a shows the Nye tensor of the relaxed a/2[111] edge dislocation core in the model $Co_{16.67}Fe_{36.67}Ni_{16.67}Ti_{30}$ alloy, again for 3b-thick sections along the dislocation line at 0 and +/-50b

along the dislocation line. The edge dislocation core is planar at most of the sections along the dislocation line, which is not surprising since moving out of plane requires some climb. However, there are some sections where the core appears spread on successive (-110) planes and so is non-planar. Unlike the screw dislocation, the center of the core shifts along the glide plane, i.e. the initial dislocation is wavy in the glide plane, as postulated to occur for edge dislocations in FCC HEAs [7]. This is also seen in the top view of the edge dislocation shown in Figure 4b, where again, atoms with a coordination number other than the bcc coordination of 14 is shown. Figure 5 shows the edge dislocation core in the mean-field A-atom material (differential displacement plot), exhibiting the dissociation into two partials separated by a stacking fault that is typical of predictions in elemental BCC metals using other interatomic potentials. The average dissociation distance is comparable to those measured in the true random alloy.

3.2 Critical resolved shear stress for the screw dislocation

The screw dislocation in the random alloy is found to move significantly (> 20A) between applied shear stresses of 0.035 and 0. 04μ at 0K, where μ is the 111 shear modulus (39 GPa), a very high Peierls barrier , similar to bcc metals. The high Peierls barrier is assumed to have it's origin in the non-planarity of the core as well as solute interactions at the dislocation core. Figure 6 shows the measured critical resolved shear stress necessary to achieve on-going glide as a function of temperature, for the screw dislocation. The upper and lower bounds of the critical resolved shear stress is shown in the plot. The decrease in strength with increasing temperature is relatively slow, with a drop of only ~30% between T=5K and T=300K; this indicates a high activation energy for thermally-activated motion (see below). Also shown in Figure 4 is the measured strength for the mean-field A-atom material as a function of temperature scaled by the 111 shear modulus (44 GPa). The strength of the mean-field material is much lower, less than 50% of the true random alloy, at T=5K. This comparison explicitly shows that significant strengthening in the true random alloy arises strictly from compositional fluctuations, since the mean-field material has all the same key properties as the random material. Furthermore, the strength of the A-atom material decreases much faster with increasing temperature, with a drop of ~75% at T=300K. At T=300K, the true random alloy is thus approximately 6 times stronger than its mean-field version. The effective activation energy is thus also dominated by compositional

fluctuations in the random alloy. This comparison further shows that the strengthening in the true random alloy is not simply due to some particular average properties of the alloy, (e.g. a higher or lower unstable stacking fault, elastic moduli, or lattice constants).

The comparison of true random alloy and mean-field alloy properties does not identify a specific mechanism by which the compositional fluctuations increase the strength and effective activation energy. However, the observations in Figure 2 indicate that the compositional fluctuations lead to a varying core structure, and some of the observed core structures would require high stresses to achieve glide, consistent with our findings on the measured strength. This is further supported by observation of the screw dislocation just prior to the onset of continued gliding. Specifically, Figure 7 shows Nye tensor plots of the a/2<111> screw dislocation core at different points along the dislocation line, with centers of 0 and +/-50b, at T=300K and at an applied stress of 0.02μ just below the critical resolved shear stress. At this stage, the screw dislocation shows many kinks in the glide plane, extending over a range of distances at different positions along the dislocation line. In order to reach this configuration kinks on several (110) and (112) planes along the dislocation line would be required. This is presumed to be due to core structure variations along the dislocation line, some of which act as pinning points either preventing lateral kink motion or double-kink nucleation. Collision of the various (1-10) and (11-2) kink segments along the dislocations line will produce jogs, which in classical BCC solid solution theory have been called superjogs, which are highly immobile [20,21]. The structure is entirely different from that observed in an elemental BCC metal or in the A-atom material, where there is simple double-kink nucleation followed by lateral kink motion to advance the dislocation by one unit, with nucleation events widely separated in time so that the dislocation remains quite straight. Finally, also shown in Figure 4 are simulations of the strength scaled by the 111 shear modulus (83 GPa) for the a/2<111> screw dislocation in BCC Fe using the Mendelev potential [19,22]. The strength of the HEA alloy, particularly the true random alloy, is far higher than that for Fe and with a much larger effective activation energy.

We have mentioned above an “effective kink pair activation energy” for the screw dislocation motion. We now quantify the discussion by fitting a standard BCC kink-pair model to the MD data [23]. For the kink-pair model, the kink-pair activation energy $\Delta H(\tau)$ at an applied stress τ is written as

$$\Delta H(\tau) = \Delta H_0 (1-(\tau/\tau_0)^p)^q \quad (1)$$

where τ_0 is the T=0K critical resolved shear stress and p=0.5 and q=2 emerge from the fit [23,24]. The double-kink nucleation rate is then given by the Arrhenius law

$$\nu_{DK} = \nu_0 \exp(-\Delta H/kT) \quad (2)$$

where ν_0 is an attempt frequency. At a constant applied stress τ imposed for a specified time t, the probability of double-kink nucleation per nucleation site is $P(\tau)\sim\nu t$. The mean time for nucleation along a line having N independent nucleation sites then satisfies $P(\tau)=1/2N$, and thus the stress required to achieve nucleation in time t can be determined as

$$\tau = \tau_0(1.0-(kT\ln(2N\nu_0 t)/\Delta H_0)^{0.5})^{2.0} = \tau_0(1.0-CT^{0.5})^{2.0} \quad (3)$$

where

$$C = [k \ln(2N\nu_0 t)/\Delta H_0]^{0.5} \quad (4)$$

Neglecting the time for lateral kink motion, as usually done, the apparent average glide velocity of the dislocation is then $v\sim b/t$. A macroscopic strain rate at a given dislocation density could then be estimated using Orowan's law $d\varepsilon/dt = \rho_m b v$, but this does not pertain to MD simulations of individual dislocations. Fitting Eq. 3 to the simulation data for the true random alloy, the mean-field alloy and Fe, as indicated in Figure 6, we obtain $C=0.011-0.0127K^{-0.5}$, $0.030 – 0.039K^{-0.5}$, and $0.058 – 0.070K^{-0.5}$ respectively. Taking N as ~ 100, $\nu_0 \sim 5 \times 10^{13}$/s, t = 100 ps, one gets for Fe, $\Delta H_0 \sim 0.25 – 0.35$ eV. These values compare favorably with a direct atomistic simulation of kink-pair activation energy for infinite separation distances for the Mendelev Fe potential, 0.6 eV [25]. Similarly, the kink-pair activation energy for the mean-field alloy and the true random alloy are determined to be 0.75 -1.28 and 7.25 – 9.89 eV, from equation (4). . The larger value of ΔH_0 for the homogeneous alloy reflects differences in the atomic-level material properties between Fe and the homogeneous BCC alloy. The much larger value of ΔH_0 in the true random alloy demonstrates clearly that local fluctuations in concentration and/or local core structure create very large activation energies, a factor of ~9 larger than in the mean-field alloy of the exact same composition. This analysis assumes that the double-kink nucleation model applies to the true random alloy, and so the quantitative comparison should not be taken as definitive. We have

shown (Figure 7) that the dislocation in the random alloy is highly kinked, suggesting that kink nucleation is not difficult everywhere, and that the strength may be controlled by lateral kink motion and/or by pinning of the dislocation by local core structures that are very unfavorable for glide. Independent of the detailed mechanisms, which require further investigation, the random alloy has a much larger effective activation energy for glide as evidenced by the direct MD simulation data in Figure 6.

3.3 Critical resolved shear stress for the edge dislocation

For a/2<111> edge dislocations in pure BCC Fe with the Mendelev potential, the Peierls stress at 0K is extremely small, < 10 MPa and the core structure of the edge dislocations was planar as in the homogeneous alloy. The critical stress to move the edge dislocations in the homogeneous alloy was also very small, < 10 MPa. Such low values are typical of edge dislocations in BCC metals, and give rise to the huge screw/edge anisotropy in apparent mobility, leading to dominance of screw dislocations in the deformation of BCC metals. In the true random alloy, the situation is rather different. Figure 8 shows the critical resolved shear stress versus temperature as obtained from the MD results for the motion of the a/2<111> edge dislocations in the random alloy. The CRSS is several orders of magnitude higher than the T=0K CRSS for the homogeneous alloy and BCC Fe. The dislocation core remains largely planar, however there is a tendency for the edge dislocation core to become non-planar at certain points along the dislocation line due to compositional fluctuations in the random alloy (Figure 4) and so the strengthening arises from the overall interactions of the randomly-distributed atoms with the dislocation as it moves through the material. This high strengthening, relative to an elemental or average-atom material, is similar to that found in FCC metals [7], where the strengthening has been directly tied to solute-dislocation interactions in a concentrated solid solution. We thus expect the mechanism of strengthening of the BCC edge to be similar.

The strengthening of the edge in the random alloy changes the screw/edge anisotropy in a significant way. At room temperature (T=300K), the CRSS for the screw is 0.02-0.25μ and 0.01-0.015μ for the edge. The ratio is thus approaching unity, as compared to a ratio of ~100 in the elemental and average-atom BCC materials. The effect of the random alloy is thus not only to strengthen the material significantly, and to increase the activation energy that controls the flow strength, but also to make the material more isotropic with respect to screw/edge motions. The

BCC HEA alloy thus becomes more like an FCC material, although the detailed mechanisms of dislocation motion for the screw likely remain different between BCC and FCC.

5. Conclusions

Dislocation behavior in a BCC $Co_{16.67}Fe_{36.67}Ni_{16.67}Ti_{30}$ alloy has been modeled. The equilibrium a/2<111> screw dislocation core structure in the true multi-component random alloy shows significant core structure variations along the dislocation line, presumably associated with concentration fluctuations that change the local stacking fault energies on different possible slip planes. The stresses (CRSS) required to move these dislocations are much larger than in a homogeneous version of the same alloy composition, demonstrating that the random nature of the alloy increases strength. One aspect of this strengthening is frequent formation of superjogs along the moving dislocation, a mechanism that is not expected in ether elemental BCC metals or the mean field model of the disordered alloy. The temperature dependence of the CRSS is also much weaker than in the mean-field alloy or element BCC Fe, indicating that the random alloy creates significantly larger energy barriers to dislocation motion. This is reflected in direct observations of a complex dislocation structure in the MD simulations.

In the model BCC HEA, the Ti atom is a strong misfit strain center, and this could lead to the observed core structure variations along the dislocation line for both a/2[111] screw and edge dislocations. Real refractory BCC high entropy alloys have much lower misfit strain centers [8,9], and so the effects seen here may be reduced. However, even in these alloys, the propensity of the screw dislocation to kink on different planes along the dislocation line is expected because of local concentration fluctuations, and this should lead to the relatively high effective kink-pair activation energy as observed in the model alloy. Furthermore, the CRSS for the edge dislocation is comparable to that for the screw, which is highly atypical as compared to elemental BCC metals. This has implications for higher-scale modeling (dislocation dynamics or crystal plasticity) of HEA alloys, relative to elemental BCC metals, which may lead to enhanced overall performance in polycrystalline HEA materials.

Acknowledgement

The authors acknowledge use of the Molecular dynamics code LAMMPS, which was developed at Sandia National Laboratory by Dr. Steve Plimpton and co-workers. This work was supported by the AFOSR, and by a grant of computer time from the DOD High Performance Computing Modernization Program, at the Aeronautical Systems Center/Major Shared Resource Center. SR, WAC, and CV acknowledge support for this work by the European Research Council through the Advanced Grant ``Predictive Computational Metallurgy", ERC Grant agreement No.339081 - PreCoMet. Work by ONS and TAP was supported through the Air Force onsite contract No. FA8650-15-D-5230 managed by UES, Inc.

References:

1) F.C. Campbell, 'Phase Diagrams – Understanding the Basics', ASM International, 2012.
2) S. Curtarolo, Nature Materials, **12** (2013) 191.
3) B.S. Murty, J.W. Yeh and S.Ranganathan, 'High Entropy Alloys', Butterworth-Heinemann, 2014.
4) M. Poletti and L. Battezzati, Acta Mater., **75** (2014) 297.
5) J.W. Yeh et.al., Metall.Mater.Trans., **35A** (2004) 2533.
6) J.W. Yeh et.al., Adv.Engr.Mater., **6** (2004) 299.
7) C. Varvene, AND OTHERS, Acta Materialia, submitted (2016).
8) O.N. Senkov, G.B. Wilks, D.B. Miracle, C.P. Chuang and P.K. Liaw, Intermetallics, **8** (2010) 1758.
9) O.N. Senkov, G.B. Wilks, J.M. Scott and D.B. Miracle, Intermetallics, **19** (2011) 698.
10) O.N. Senkov, J.M. Scott, S.V. Senkova, D.B. Miracle and C.F. Woodward, J.Alloys.Compounds, **509** (2011) 6043.
11) X.W. Zhou et.al., Acta Mater., **49** (2001) 4005.
12) www.ctcms.nist.gov/potentials/
13) S.J. Plimpton, J. Comput. Phys., **117** (1995) 1.

14) Bower, Claridge and Tsong, Phys.Stat.Solidi., **29** (1968) 617.

15) M.R. Fellinger, PhD thesis, Graduate program in Physics, The Ohio State University, 2013.

16) C.S. Hartley and Y. Mishin, Acta.Mater., **53** (2005) 1313.

17) V. Vitek, R.C. Perrin and D.K. Bowen, Phil.Mag., **21** (1970) 1049.

18) C. Varvenne et.al., PUBLISHED IN PHYS. REV.

19) T. Chaussidon, M. Fivel and D. Rodney, Acta Mater., **54** (2006) 3407.

20) A.S. Argon in 'Strengthening Mechanisms in Crystal Plasticity', Oxford series on Materials Modeling, Oxfor University Press, Oxford, UK, 2008, 174.

21) H.Suzuki in 'Disloactions in Solids', v4, edited by F.R.N. Nabarro, North Holland, Amsterdam, 191.

22) M.I. Mendelev et.al., Phil. Mag., **83** (2003) 3977.

23) U.K. Kocks. A.S. Argon and M.F. Ashby, Prog.Mater.Sci., **19** (1975) 1.

24) D. Rodney and J. Bonneville in 'Physical Metallurgy – 5th edition' D.E. Lauglin and K. Hono editors, 2015, Elsevier.

25) M.R. Gilbert, S. Queyreau and J. Marian, Phys.Rev.B **84** (2011) 174103.

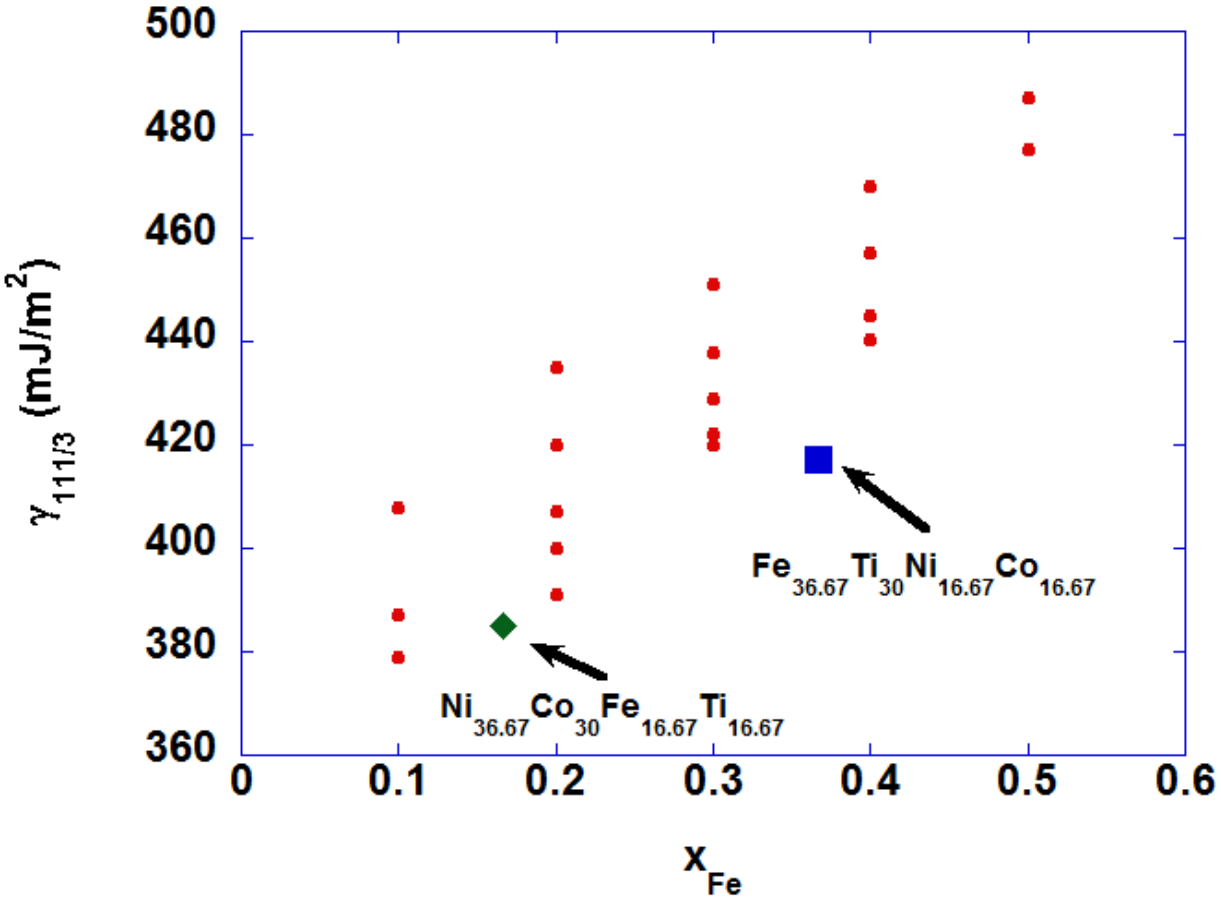

Fig.1:

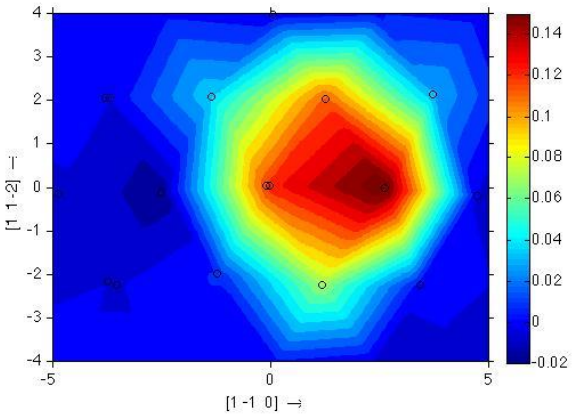

-30b

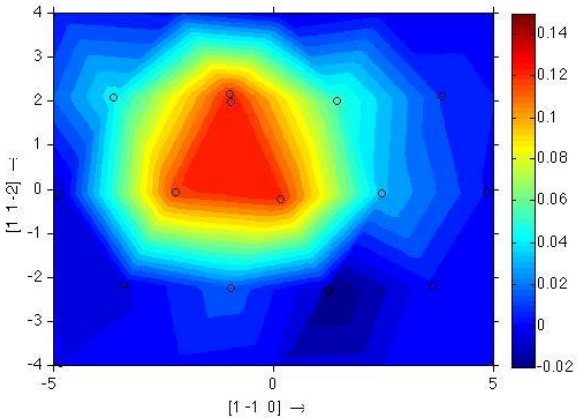

0b

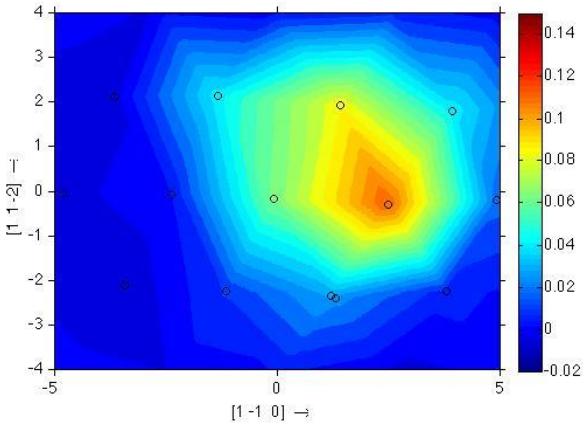

30b

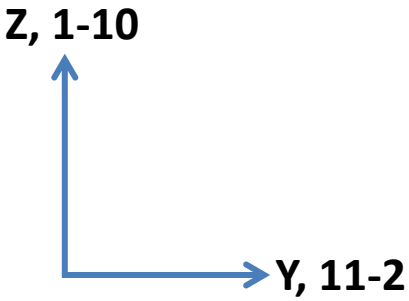

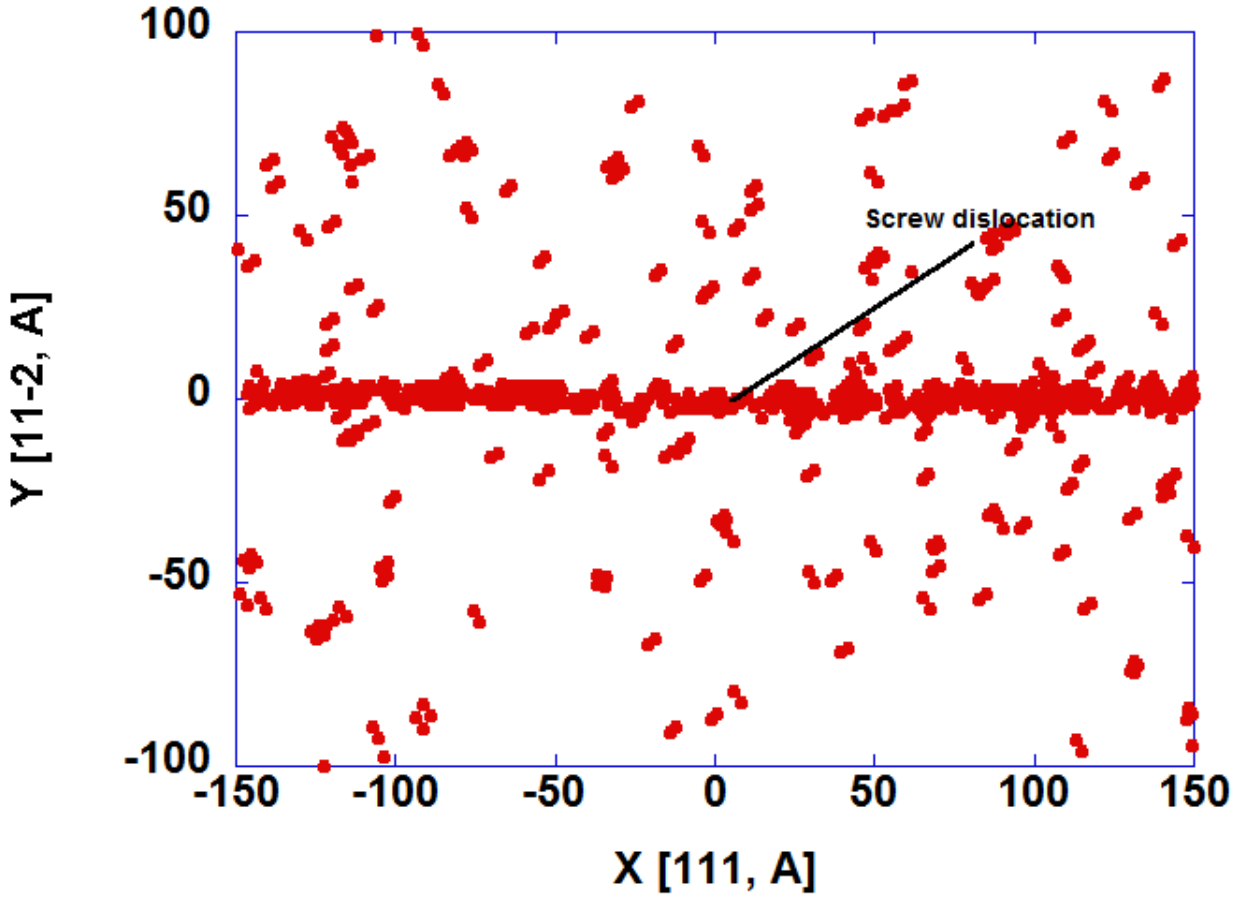

Fig.2b:

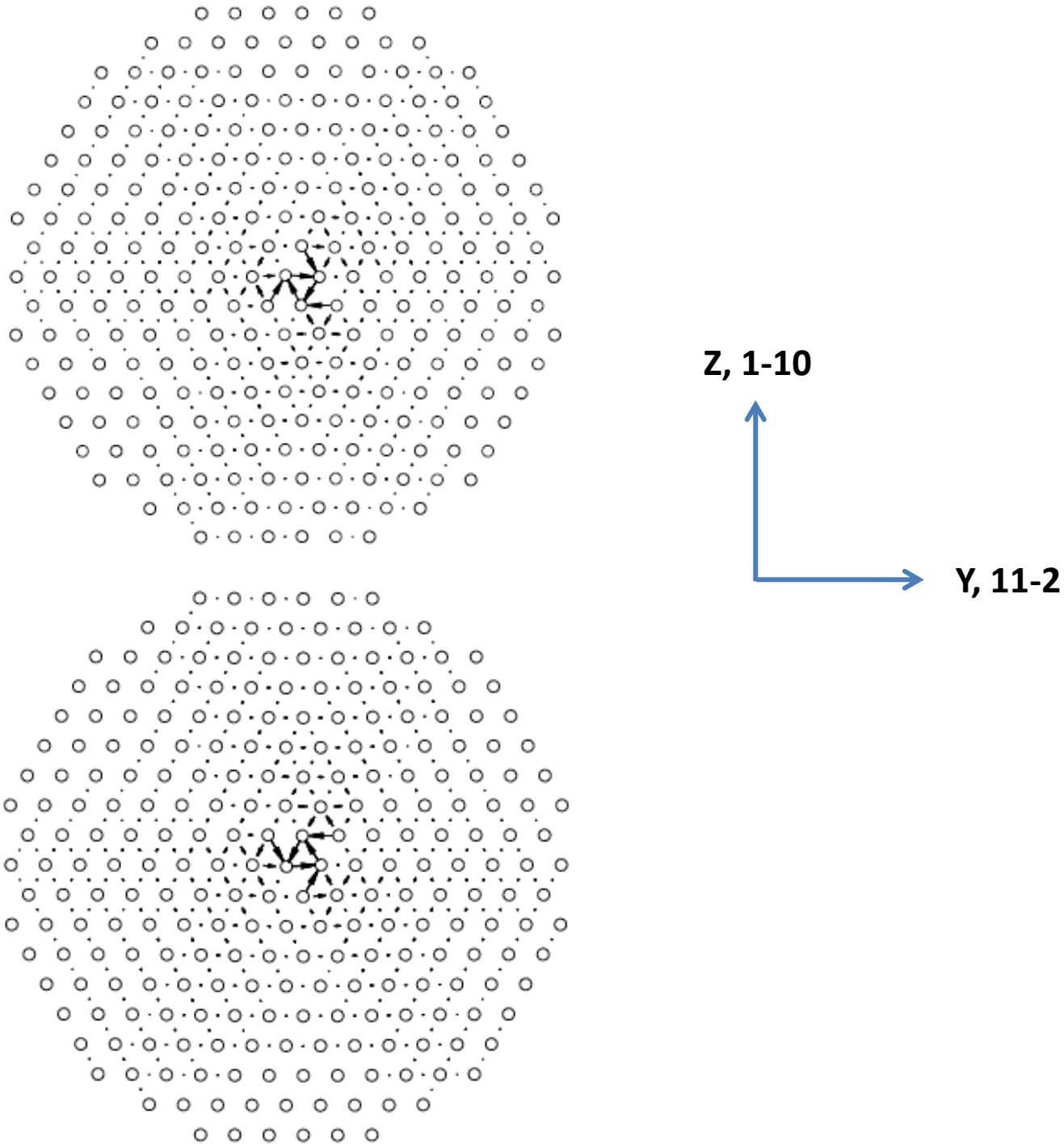

Fig. 3:

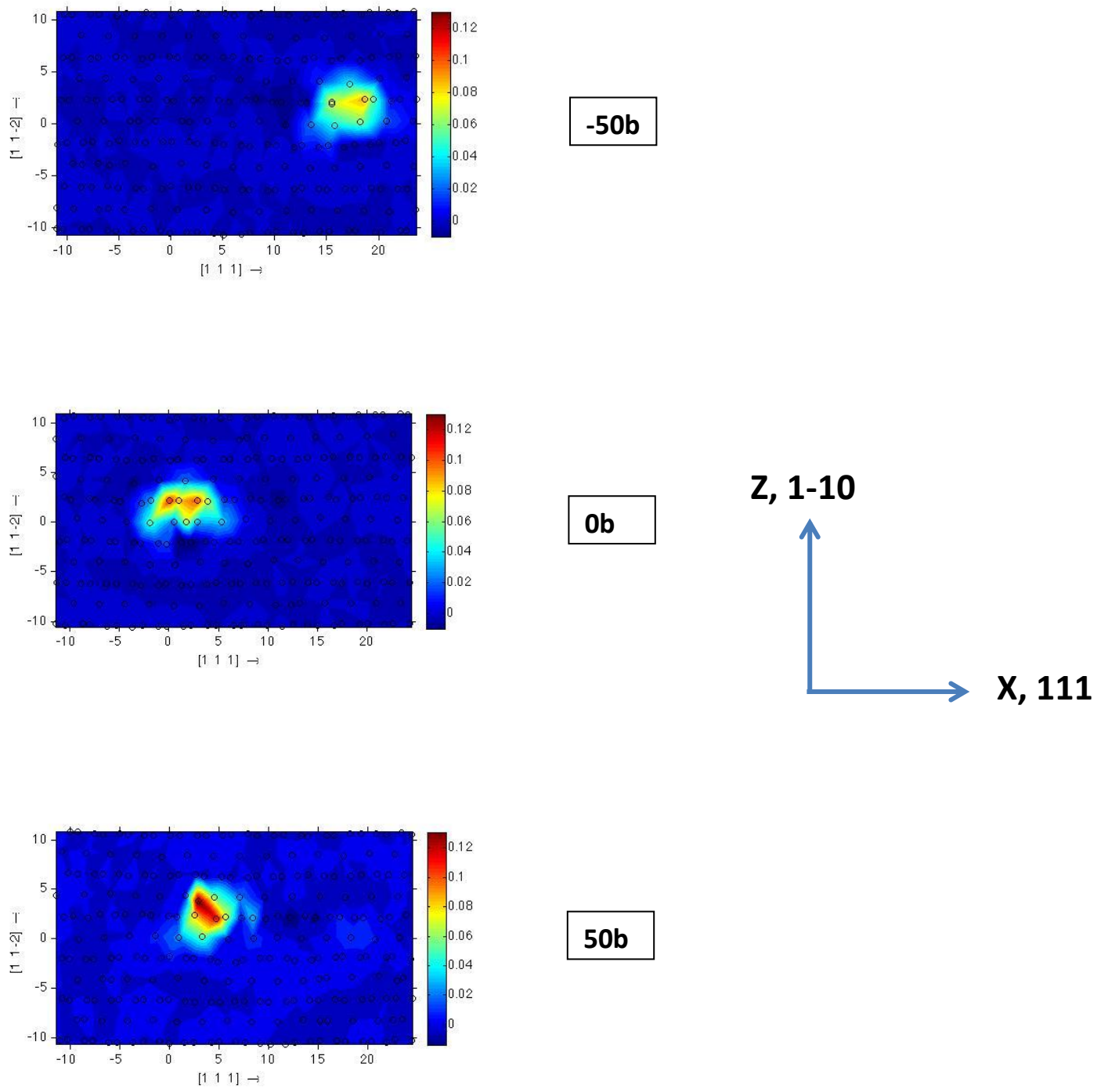

Fig.4a:

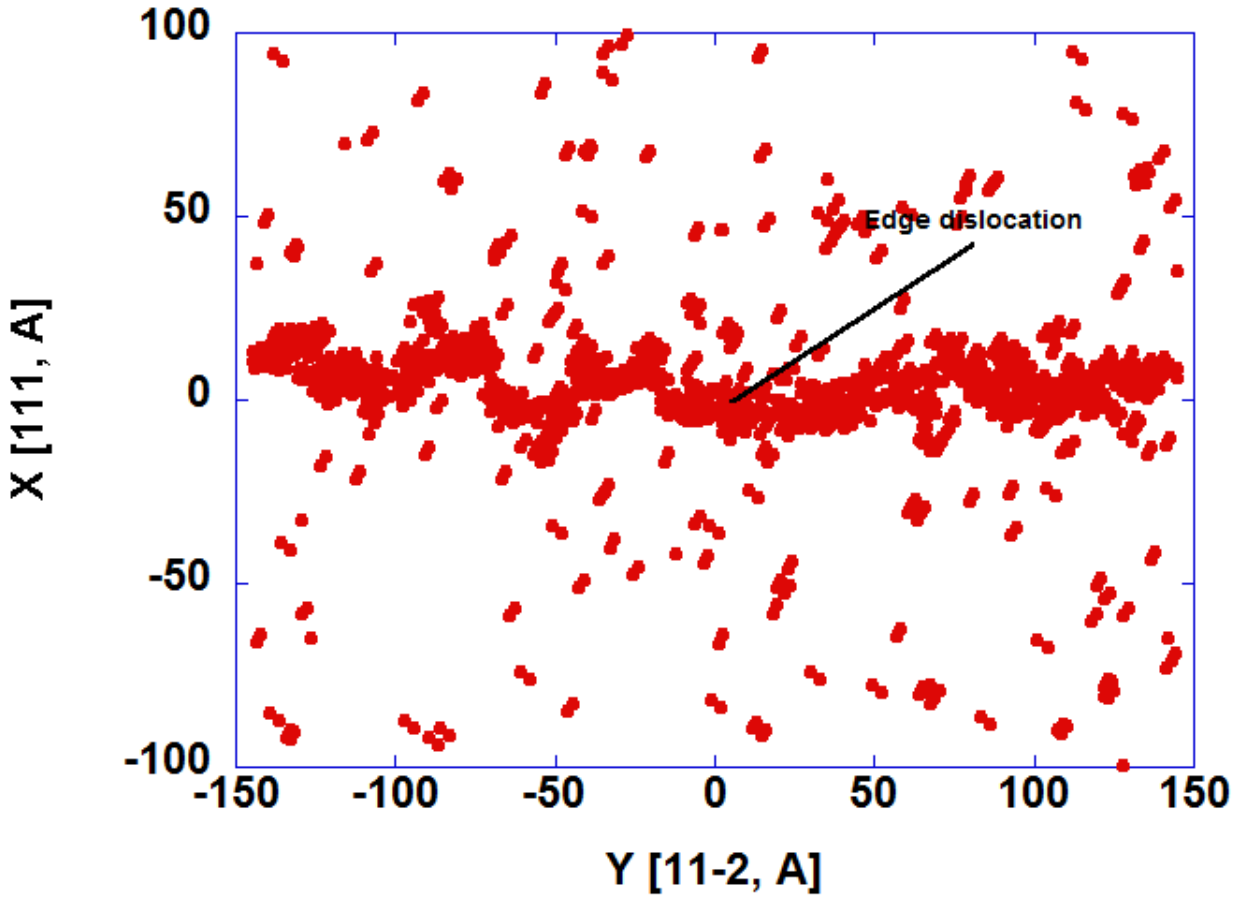

Fig.4b:

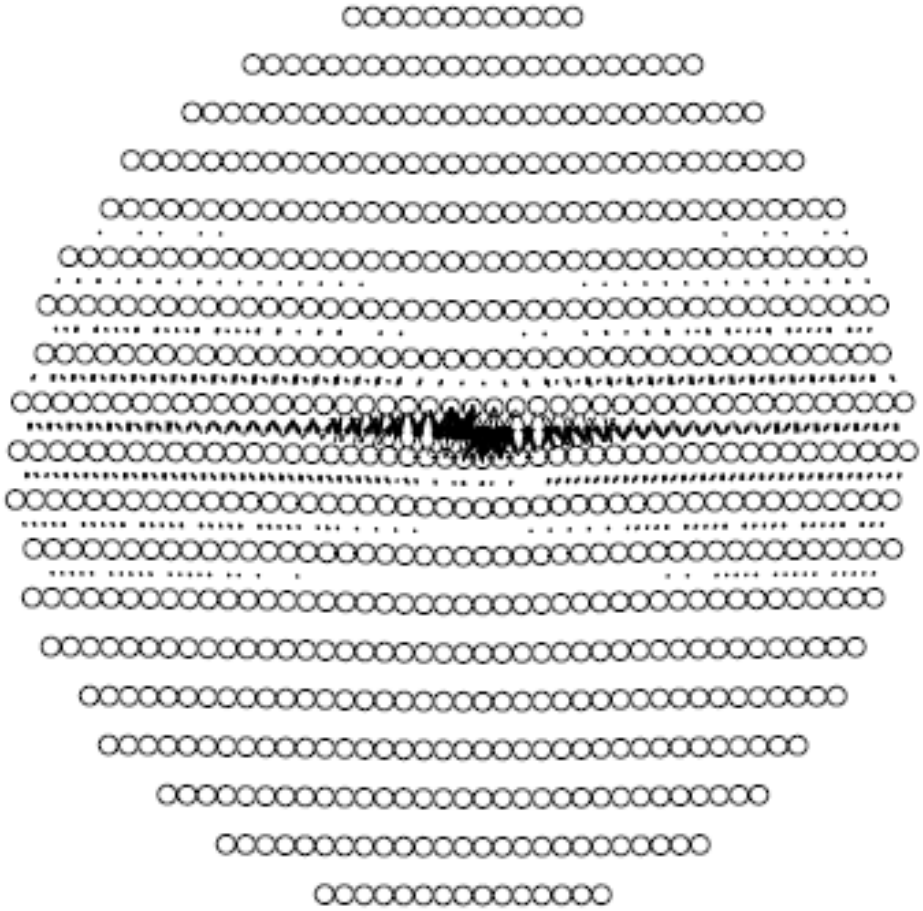

Fig.5:

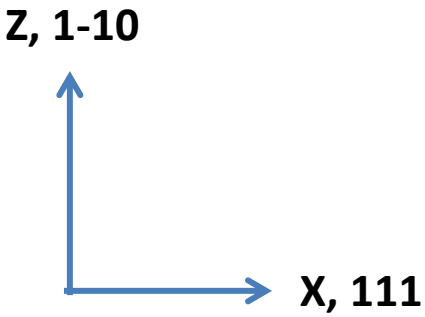

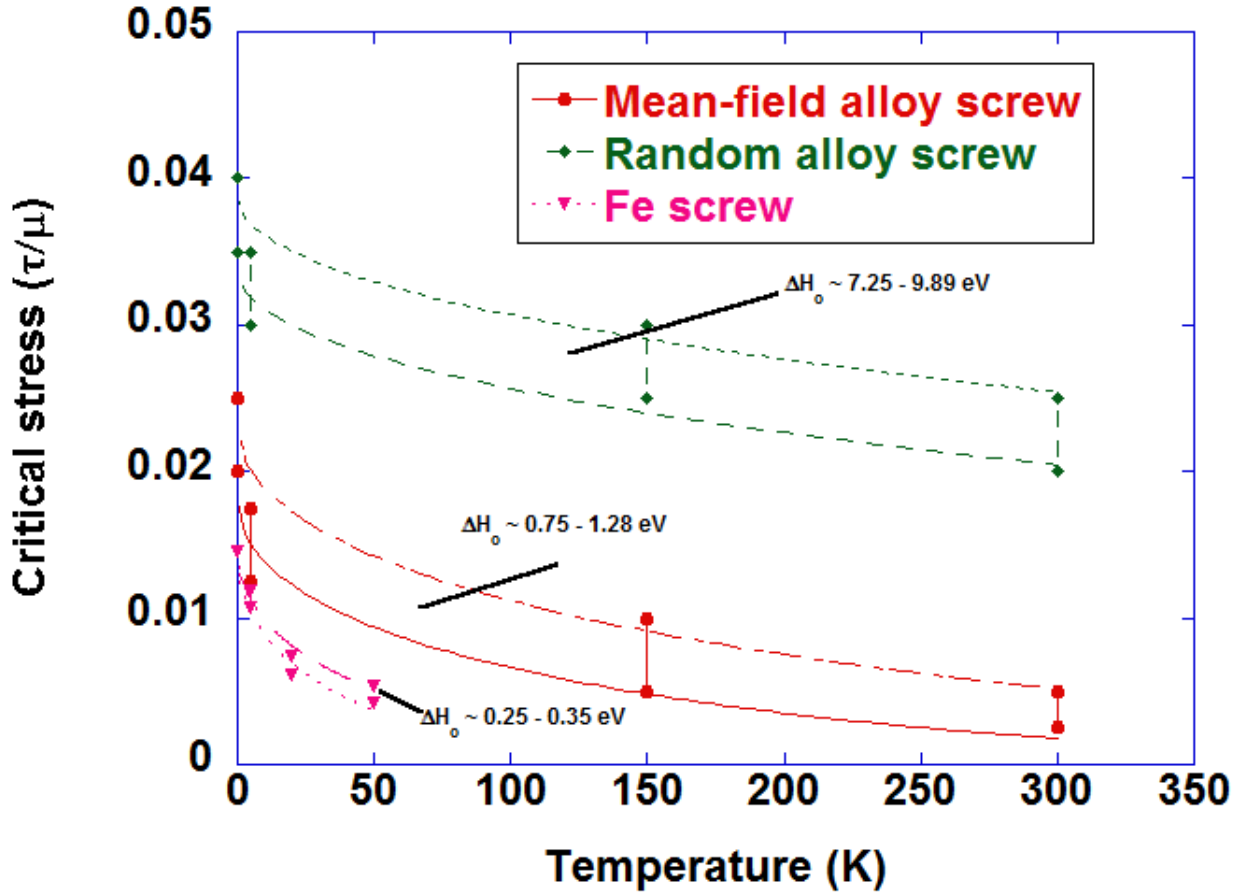

Fig.6:

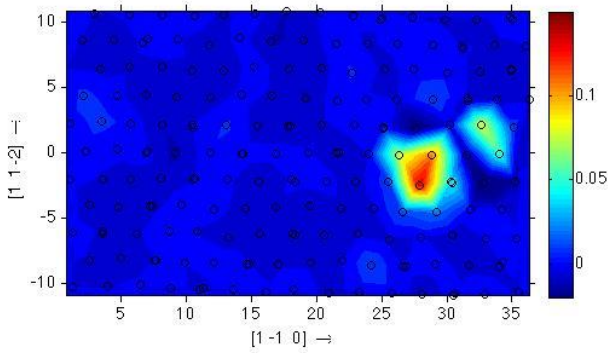

-50b

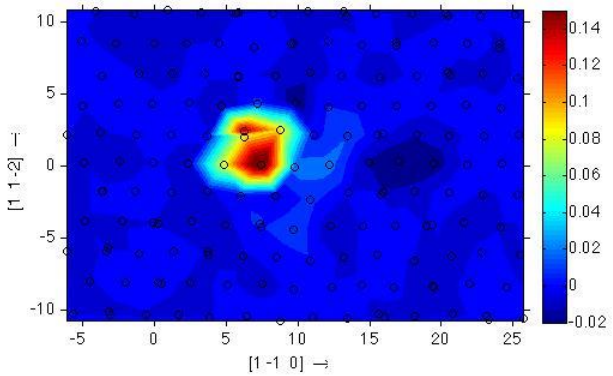

0b

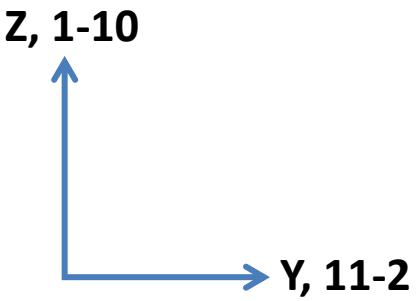

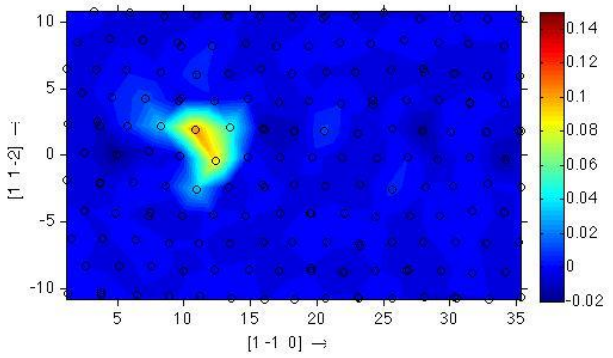

50b

Fig.7:

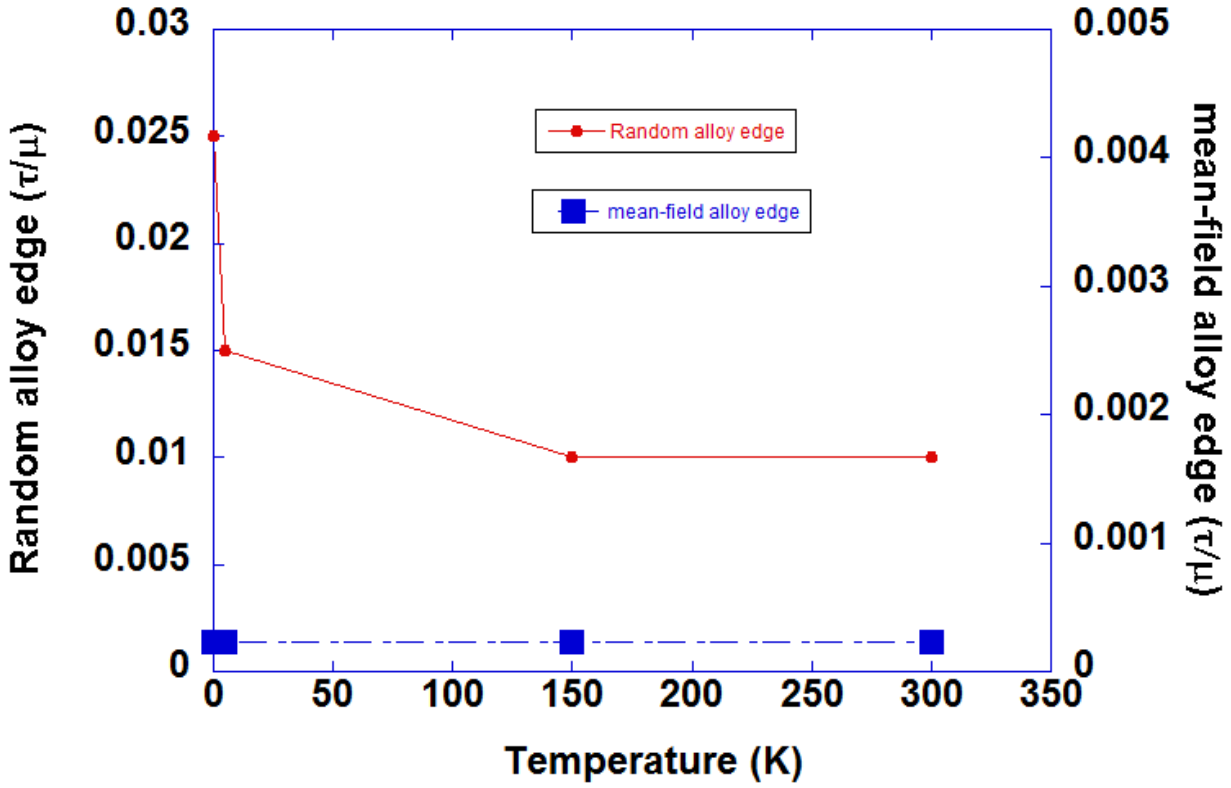

Fig.8: